Dense Multipath Component Polarization and Wall Attenuation at 1.35 GHz in an Office Environment

E. Tanghe[1], P. Laly[2], D. P. Gaillot[2], N. Podevijn[1], S. Denis[3], N. BniLam[3], B. Bellekens[3], R. Berkvens[3], M. Weyn[3], M. Liénard[2], L. Martens[1], and W. Joseph[1]
[1]IMEC-WAVES, Ghent University, Ghent, Belgium, emmeric.tanghe@intec.ugent.be
[2]IEMN-TELICE, University of Lille 1, Lille, France, davy.gaillot@univ-lille1.fr
[3]IMEC-IDLab, University of Antwerp, Antwerp, Belgium, maarten.weyn@uantwerpen.be

***Abstract*—This paper presents an analysis of dense multipath components in office meeting rooms. Radio channel sounding measurements at 1.35 GHz were performed with transmitter and receiver in the same room (intra-room) and in adjacent rooms (inter-room). Specular and dense multipath components were estimated with the RiMAX maximum-likelihood algorithm. The dense multipath reverberation characteristics were found to be not significantly different between polarization subchannels for both the intra-room and the inter-room channels, supporting the validity of a scalar dense multipath model. The specular and dense multipath wall attenuation losses were found to be 12.0 and 5.4 dB, respectively.**

***Index Terms*—channel sounding, RiMAX, dense multipath, specular multipath, polarization, wall attenuation, office**

I. Introduction

This work analyses the dependency of dense multipath reverberation on polarization state. The analysis is based on radio channel sounding measurements at 1.35 GHz in two adjacent office meeting rooms. The sounding data is processed with the RiMAX estimator to split the radio channel into specular multipath components (SMCs) and dense multipath components (DMC) [1]. The SMCs have well-defined discrete locations in the different radio channel dimensions (space, frequency, and time) and originate mostly from diffractions and specular reflections. The DMC are the part of the radio channel that is continuous across the channel dimensions. Among other sources, the DMC originate from distributed diffuse scattering on electrically small objects [2].

The parameter of interest in this study is the DMC reverberation time τ_r. We investigate whether τ_r depends on the polarization state of transmitter and receiver, or if τ_r originates from the same population (distribution) independent of polarization state. We found one study at 2.3 and 5.8 GHz inside a seminar room that did not observe a significant change in reverberation time with polarization state [3]. In [3], the reverberation time was determined through visual inspection of the tail of the power delay profile. In our work, we perform a more rigorous separation of specular and dense multipath by making use of the RiMAX estimator. The RiMAX algorithm provides us with a more objective and thus robust estimate of the reverberation time. In contrast to [3], we also performed a reverberation time analysis for the transmitter and receiver not in the same room. Finally, we also estimated the wall attenuation loss experienced by the SMCs and DMC separately. The DMC wall attenuation loss is useful for calculating the wall resistance in circuit models of DMC propagation [4].

II. Measurements

A. Equipment

Measurements were performed with the MIMOSA radio channel sounder [5], [6]. Its transmission bandwidth is 80 MHz centered around a carrier frequency of 1.35 GHz. The sounder consists of a transmitter (Tx) and a receiver (Rx) having 8 and 16 channels, respectively. The 8×16 sounder is fully parallel: the data from each transmit antenna is simultaneously modulated onto the carriers with a frequency interleaving technique (Interleaved Frequency Division Multiple Access or IFDMA). Each transmit channel is connected to a two-port RF switch, thereby increasing the number of transmit channels to 16 at the cost of channel acquisition time. The 16 channels at each link end are distributed over a vertical planar antenna array consisting of $M_R = M_T = 8$ dual-polarized patches (having a horizontal (H) and a vertical (V) polarization). Fig. 1 shows the patch antenna array used at both Tx and Rx.

Orthogonal Frequency Division Multiplexing (OFDM) is used to encode the digital transmit symbols. The 80 MHz bandwidth is divided into 6560 subcarriers, equally divided between the 8 parallel transmit channels. This results in an

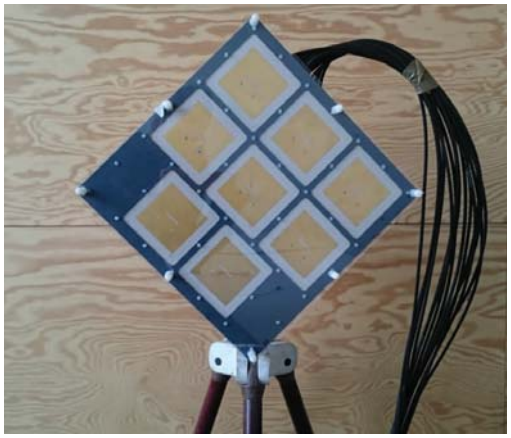

Fig. 1. Dual-polarized patch antenna array

interfrequency spacing of 12.21 kHz and an OFDM symbol duration T_S of 81.92 µs. The duration of the cyclic prefix T_{CP} can be chosen as a fraction of T_S. For the multipath estimation, only $M_f = 103$ subcarriers were retained to keep the estimation reasonably fast. Taking into account the two-state RF switch at the Tx, the acquisition of one 16×16 channel snapshot takes up at most 327.68 µs. Table I summarizes the technical specifications of MIMOSA.

TABLE I
MIMOSA SPECIFICATIONS

parameter	setting
center frequency	1.35 GHz
bandwidth	80 MHz
number of Tx antennas	8
number of Rx antennas	8
Tx polarization	H/V
Rx polarization	H/V
number of OFDM subcarriers	6560
OFDM symbol duration T_S	81.92 µs
cyclic prefix duration T_{CP}	$0 \leq T_{CP} \leq T_S$
16×16 channel acquisition time	$2\,(T_S + T_{CP}) \leq 327.68$ µs
transmit power per Tx channel	0.1-1 W

B. Procedure

Fixed-link radio channels were recorded in two office-type meeting rooms. Fig. 2 shows a floor plan of both rooms and the adjacent hallway. The dimensions of room 1 are $9.47 \times 6.83 \times 4.00$ m^3, while room 2 measures $4.68 \times 6.83 \times 4.00$ m^3. The floor and ceiling are made of concrete. The outer wall (top in Fig. 2) is made up of concrete structures and windows, while all the inner walls are plasterboard. Meeting tables and chairs were the only inventory in both rooms.

Fig. 2 also shows the four positions of Tx array (red) and the five locations of the Rx array (blue) chosen for the measurements. The antenna arrays were positioned parallel to the walls and radiated towards the inside of the room they are in. The radio channel was recorded between each Tx and each Rx position for a total of 20 radio links. Each radio channel was measured 50 times in static conditions and averaged to reduce measurement noise.

III. DATA MODEL

The vectorized channel gain $\boldsymbol{h}_{XY} \in \mathbb{C}^{M_R M_T M_f \times 1}$ can be written[1] as the sum of an SMC part $\boldsymbol{s}_{XY}$, a DMC part $\boldsymbol{d}_{XY}$, and a measurement noise part $\boldsymbol{n}_{XY}$:

$$\boldsymbol{h}_{XY} = \boldsymbol{s}_{XY}\left(\boldsymbol{\Theta}_{s,XY}\right) + \boldsymbol{d}_{XY}\left(\boldsymbol{\theta}_{d,XY}\right) + \boldsymbol{n}_{XY}\left(\sigma^2_{XY}\right) \quad (1)$$

It is assumed that $\boldsymbol{h}_{XY}$ follows a multivariate circularly symmetric complex Gaussian distribution:

[1]The subscripts X and Y denote the polarization of the transmitting and the receiving antenna, respectively. X and Y are either horizontal (H) or vertical (V).

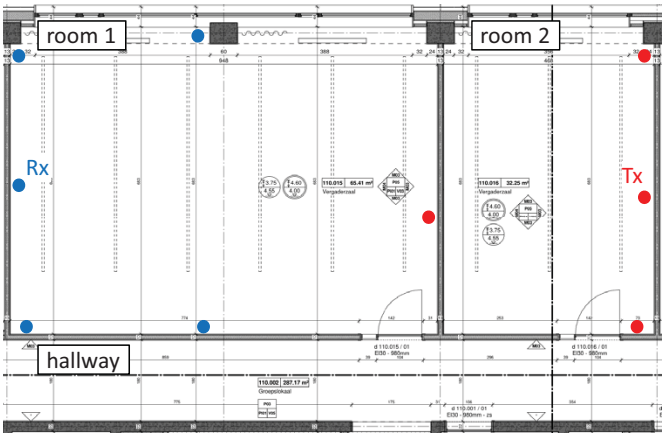

Fig. 2. Floor plan with locations of the Tx and Rx arrays

$$\boldsymbol{h}_{XY} \sim \mathcal{N}_c\Big(\boldsymbol{s}_{XY}\left(\boldsymbol{\Theta}_{s,XY}\right), \boldsymbol{R}_{XY}\left(\boldsymbol{\theta}_{d,XY}, \sigma^2_{XY}\right)\Big) \quad (2)$$

A. Specular multipath components

The parameter matrix $\boldsymbol{\Theta}_{s,XY}$ groups the parameters associated with the SMCs:

$$\boldsymbol{\Theta}_{s,XY} = \begin{bmatrix} \boldsymbol{\varphi}_A \\ \boldsymbol{\vartheta}_A \\ \boldsymbol{\varphi}_D \\ \boldsymbol{\vartheta}_D \\ \boldsymbol{\tau}_A \\ \boldsymbol{\gamma}_{XY} \end{bmatrix} \begin{array}{l} \leftarrow \text{azimuth of arrival} \\ \leftarrow \text{elevation of arrival} \\ \leftarrow \text{azimuth of departure} \\ \leftarrow \text{elevation of departure} \\ \leftarrow \text{time of arrival} \\ \leftarrow \text{complex amplitude} \end{array} \quad (3)$$

In (3), $\boldsymbol{\Theta}_{s,XY}$ is a $6 \times N$ matrix where N is the number of specular multipath components. Each row of $\boldsymbol{\Theta}_{s,XY}$ contains the corresponding specular parameter for each of the N specular paths. The SMC part $\boldsymbol{s}_{XY}$ is then calculated as [1]:

$$\begin{aligned} \boldsymbol{s}_{XY}\left(\boldsymbol{\Theta}_{s,XY}\right) = \Big[& \left(\boldsymbol{G}_{R,Y}\left(\boldsymbol{\varphi}_A, \boldsymbol{\vartheta}_A\right) \circ \boldsymbol{A}_R\left(\boldsymbol{\varphi}_A, \boldsymbol{\vartheta}_A\right)\right) \\ & * \left(\boldsymbol{G}_{T,X}\left(\boldsymbol{\varphi}_D, \boldsymbol{\vartheta}_D\right) \circ \boldsymbol{A}_T\left(\boldsymbol{\varphi}_D, \boldsymbol{\vartheta}_D\right)\right) \\ & * \boldsymbol{A}_f\left(\boldsymbol{\tau}_A\right) \Big] \boldsymbol{\gamma}^T_{XY} \end{aligned} \quad (4)$$

In (4), $\circ$ and $*$ are the Schur-Hadamard and the column-wise Khatri-Rao matrix products, respectively. $\boldsymbol{A}_R \in \mathbb{C}^{M_R \times N}$, $\boldsymbol{A}_T \in \mathbb{C}^{M_T \times N}$, and $\boldsymbol{A}_f \in \mathbb{C}^{M_f \times N}$ are Rx, Tx, and frequency steering matrices containing complex exponentials. Further, $\boldsymbol{G}_{R,Y}$ and $\boldsymbol{G}_{T,X}$ are matrices that pre-multiply the complex exponentials in the Rx and Tx steering matrices with the appropriate polarimetric antenna gains.

B. Dense multipath components and noise

The DMC $\boldsymbol{d}_{XY}$ and the noise $\boldsymbol{n}_{XY}$ in (1) are fully determined by the covariance matrix $\boldsymbol{R}_{XY}$ in (2). This covariance matrix is assumed to have the following structure involving Kronecker products [1]:

$$\boldsymbol{R}_{XY}\left(\boldsymbol{\theta}_{d,XY}, \sigma^2_{XY}\right) = \boldsymbol{I}_{M_R} \otimes \boldsymbol{I}_{M_T} \otimes \boldsymbol{R}_{f,XY}\left(\boldsymbol{\theta}_{d,XY}\right) + \sigma^2_{XY}\boldsymbol{I}_M \quad (5)$$

In (5), $\boldsymbol{I}_\kappa$ is the identity matrix of size κ and $M = M_R M_T M_f$. The measurement noise is modeled as independent and identically distributed (i.i.d.) complex Gaussian noise with variance σ^2_{XY}. The DMC is assumed to be correlated and wide-sense stationary in the frequency domain: this implies that the frequency covariance matrix $\boldsymbol{R}_{f,XY}$ has a Toeplitz structure. The exact mathematical expression of $\boldsymbol{R}_{f,XY}$ is derived from the DMC power delay profile $\psi_{XY}(\tau)$ as function of delay τ [1]. It is assumed that the DMC power delay profile follows an exponential decay with parameters grouped in the parameter vector $\boldsymbol{\theta}_{d,XY}$:

$$\boldsymbol{\theta}_{d,XY} = \begin{bmatrix} \alpha_{d,XY} \\ \tau_{d,XY} \\ \tau_{r,XY} \end{bmatrix} \begin{matrix} \leftarrow \text{peak power} \\ \leftarrow \text{onset time} \\ \leftarrow \text{reverberation time} \end{matrix} \quad (6)$$

$$\psi_{XY}(\tau) = \alpha_{d,XY} e^{-(\tau-\tau_{d,XY})/\tau_{r,XY}} \quad (7)$$

IV. RiMAX estimator

The RiMAX algorithm is applied to the channel sounding data to obtain maximum-likelihood estimates $\hat{\boldsymbol{\theta}}_{s,XY}$ and $\hat{\boldsymbol{\theta}}_{d,XY}$ of the SMC and DMC multipath parameters, and $\hat{\sigma}^2_{XY}$ of the noise variance [1]. The Effective Aperture Distribution Function (EADF) framework is used to include the polarimetric radiation patterns of the Tx and Rx antennas in the signal model [7].

The RiMAX algorithm is an iterative algorithm: in each iteration, a set of 10 SMCs is initialized with a simple multidimensional beamformer and optimized with the Levenberg-Marquardt algorithm. Subsequently, the DMC and noise, i.e., the measured channel minus all optimized SMCs, are fitted to the data model in (5) and (7). The algorithm then alternates between optimizing SMC, and DMC and noise parameters until convergence is reached. The final step in each RiMAX iteration checks the reliability of the estimated SMCs by means of a criterion based on the SMC power estimate and its estimation error variance [1], [2]. If a path fails this criterion, it is removed from the set of estimated SMCs. We set the number of RiMAX iterations to 2 for our sounding data (meaning a maximum of 20 specular paths is estimated, leaving out paths that fail the reliability criterion). With this setting, the dynamic range of the estimated SMCs was found to be around 30 dB. Setting a larger number of iterations would mainly increase the number of low-power paths that we deem untrustworthy.

Fig. 3 shows the SMC estimation for the link where the Tx is in the top right and the Rx is in the top left corner of Fig. 2. SMCs emanating from the Tx (blue dot) and impinging on the Rx (red dot) are displayed as blue and red lines, respectively. The length and thickness of the lines are proportional to the SMC path length and power, respectively.

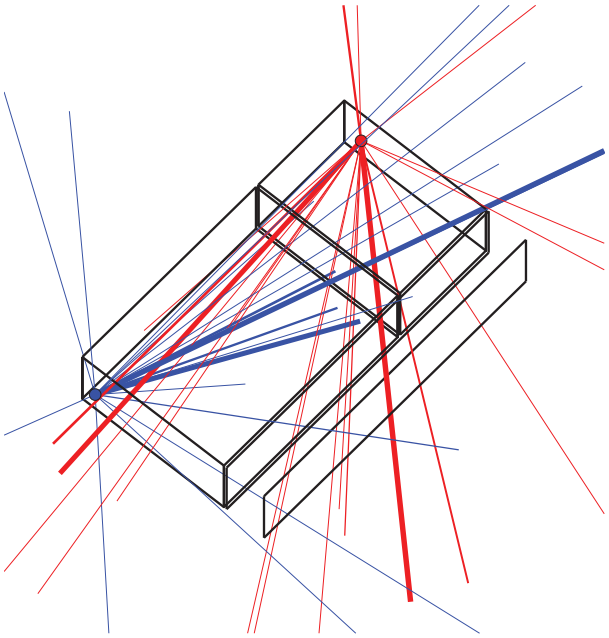

Fig. 3. SMC estimation

V. Results

A. DMC reverberation time

This section discusses the polarization-dependency of the DMC reverberation time. Fig. 4 shows reverberation time variability as boxplots. The radio links are divided into intra-room channels (Tx and Rx in room 1) and inter-room channels (Tx in room 1 and Rx in room 2). For each channel type, the reverberation times are grouped according to polarization subchannel.

We performed a Kruskal-Wallis test (i.e., a one-way analysis of variance on ranks) to find out whether there is a group effect of the polarization on the reverberation time [8]. For both the intra- and the inter-room channels, the test did not find a group effect at the 5% significance level (p-values of 0.33 and 0.09, respectively). This is evidence that the DMC in an indoor meeting room environment can be modeled as independent of polarization.

Following these findings, we modify the DMC and noise data model in Section III-B to a scalar DMC and noise model independent of polarization. In other words, we perform a fit to the total DMC and noise $\boldsymbol{d} + \boldsymbol{n}$ with

$$\boldsymbol{d} + \boldsymbol{n} = \sum_{X,Y \in \{H,V\}} \left(\boldsymbol{d}_{XY} + \boldsymbol{n}_{XY}\right) \quad (8)$$

The DMC and noise in (8) is fitted to the model in (5)-(7), but without the XY-dependency. Fig. 4 shows the variability of the reverberation times fitted to the total DMC and noise (8) as red boxplots (all).

Fig. 5 shows the power-delay characteristics of the RiMAX result (relative to the time-of-arrival of the first arriving SMC) for the same link as in Fig. 3. The black squares indicate

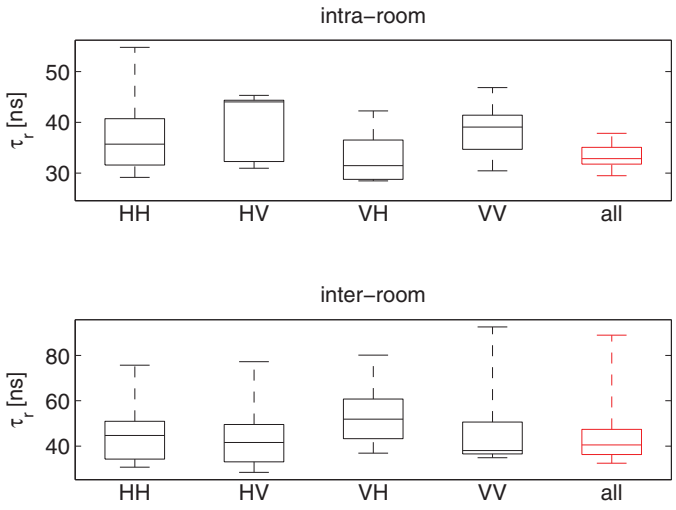

Fig. 4. Reverberation times of the intra- and inter-room channels grouped according to polarization subchannel (H = horizontal, V = vertical, first letter = Tx polarization, second letter = Rx polarization)

the powers of the discrete SMCs, the black line is the power delay profile of the measured channel and the red line is the total DMC plus measurement noise in (8). Also shown is the scalar exponential decay model fitted to the DMC + noise (green line). The RiMAX algorithm appears to have successfully separated the most powerful SMCs from the measured channel: we observe that the remaining total DMC + noise is well approximated by the scalar exponential decay model.

B. SMC and DMC attenuation loss

In this section, we estimate the attenuation loss experienced by the SMC and DMC when traveling through walls from room 2 to room 1. The DMC wall attenuation loss is used to calculate wall resistance in circuit models of DMC propagation [4]. For each Tx-Rx link, the power in the SMC (P_{SMC}) and the DMC (P_{DMC}) is calculated from the RiMAX results:

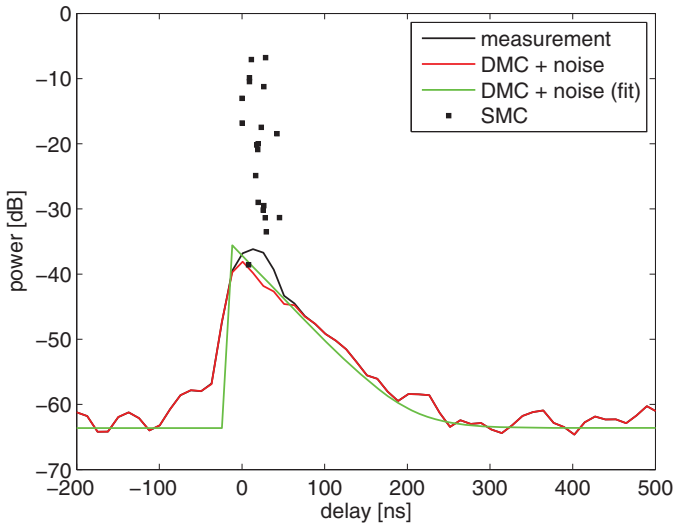

Fig. 5. Power-delay characteristics

$$P_{SMC} = \left\| \sum_{X,Y \in \{H,V\}} \gamma_{XY} \right\|^2 \tag{9}$$

$$P_{DMC} = \alpha_d \int_{\tau_d}^{\infty} e^{-(\tau-\tau_d)/\tau_r} d\tau = \alpha_d \tau_r \tag{10}$$

The attenuation loss of the SMC and DMC (A_{SMC} and A_{DMC}) is then calculated as the ratio of the median powers of the respective multipath components between the intra-room and the inter-room channels, i.e.:

$$A_{SMC/DMC} = \frac{\left[P_{SMC/DMC}\right]_{p_{50},\text{intra-room}}}{\left[P_{SMC/DMC}\right]_{p_{50},\text{inter-room}}} \tag{11}$$

We found A_{SMC} and A_{DMC} to be equal to 12.0 dB and 5.4 dB, respectively. The observation that the SMCs are more attenuated than the DMC could be explained by the SMCs commonly containing a number of paths not going through the wall shared by room 1 and 2 (see for example in Fig. 3). These paths in particular have longer travel times and go through multiple walls, causing them to be heavily attenuated. In contrast, the DMC are generally weakers paths that mostly go through the shared wall between both rooms. It is less likely that DMC passes through other walls as they would become heavily attenuated and end up in the measurement noise floor.

VI. Conclusions

In this work we presented an experimental analysis of dense multipath components at 1.35 GHz in office meeting rooms. It was found that the dense multipath reverberation characteristics are not significantly different between polarization subchannels. This implies that it is justified to use a scalar model for the sum of dense multipath components across all four polarization subchannels. Additionally, the wall attenuation loss experienced by the dense multipath appeared to be 6.6 dB smaller than the loss encountered by the specular paths. This is thought to be caused by multiple wall penetrations by some specular paths while the same is unlikely to happen for the weaker dense multipath components.

Acknowledgment

Emmeric Tanghe is a Post-Doctoral Fellow of the FWO-V (Research Foundation - Flanders, Belgium).

References

[1] A. Richter, "Estimation of Radio Channel Parameters: Models and Algorithms," Ph.D. dissertation, Technische Universität Ilmenau, Fakültat für Elektrotechnik und Informationstechnik, Ilmenau, DE, 2005.

[2] E. Tanghe, D. P. Gaillot, M. Liénard, L. Martens, and W. Joseph, "Experimental Analysis of Dense Multipath Components in an Industrial Environment," *IEEE Transactions on Antennas and Propagation*, vol. 62, no. 7, pp. 3797–3805, July 2014.

[3] J. Ø. Nielsen, J. B. Andersen, G. F. Pedersen, and M. Pelosi, "On polarization and frequency dependence of diffuse indoor propagation," in *IEEE Vehicular Technology Conference*, no. 2, San Francisco, CA, US, September 2011, pp. 1–5.

[4] A. Bamba, W. Joseph, E. Tanghe, G. Vermeeren, and L. Martens, "Circuit Model for Diffuse Multipath and Electromagnetic Absorption Prediction in Rooms," *IEEE Transactions on Antennas and Propagation*, vol. 61, no. 6, pp. 3292–3301, June 2013.

[5] P. Laly, D. P. Gaillot, E. P. Simon, M. Liénard, E. Tanghe, W. Joseph, and L. Martens, "Real-time MIMO channel Sounder based on a highly flexible Software Architecture," in *European Conference on Networks and Communications*, Paris, FR, June 2015, pp. 812–813.

[6] P. Laly, D. P. Gaillot, M. Lienard, P. Degauque, E. Tanghe, W. Joseph, and L. Martens, "Flexible real-time MIMO channel sounder for multidimensional polarimetric parameter estimation," in *2015 IEEE Conference on Antenna Measurements & Applications (CAMA)*, Chiang Mai, TH, December 2015, pp. 1–3.

[7] M. Landmann, "Limitations of Experimental Channel Characterisation," Ph.D. dissertation, Technische Universität Ilmenau, Fakültat für Elektrotechnik und Informationstechnik, Ilmenau, DE, 2008.

[8] W. H. Kruskal and W. A. Wallis, "Use of ranks in one-criterion variance analysis," *Journal of the American Statistical Association*, vol. 47, no. 260, pp. 583–621, 1952.